Field-Induced Slow Magnetic Relaxation and Gas Adsorption Properties of a Bifunctional Cobalt(II) Compound

ARTICLE *in* INORGANIC CHEMISTRY · NOVEMBER 2015

Impact Factor: 4.76

6 AUTHORS, INCLUDING:

Cai-Ming Liu

Chinese Academy of Sciences

154 PUBLICATIONS **3,064** CITATIONS

SEE PROFILE

Yi-Quan Zhang

Nanjing Normal University

52 PUBLICATIONS **349** CITATIONS

SEE PROFILE

Qing-Yan Liu

Jiangxi Normal University

55 PUBLICATIONS **799** CITATIONS

SEE PROFILE

Inorganic Chemistry

Article

pubs.acs.org/IC

Field-Induced Slow Magnetic Relaxation and Gas Adsorption Properties of a Bifunctional Cobalt(II) Compound

Yu-Ling Wang,*[,†] Lin Chen,[†] Cai-Ming Liu,[‡] Yi-Quan Zhang,[§] Shun-Gao Yin,[†] and Qing-Yan Liu*[,†]

[†]College of Chemistry and Chemical Engineering, Jiangxi Normal University, Nanchang, Jiangxi 330022, P. R. China

[‡]Beijing National Laboratory for Molecular Sciences, Institution of Chemistry, Chinese Academy of Sciences, Center for Molecular Sciences, Beijing 100190, P. R. China, and

[§]Jiangsu Key Laboratory for NSLSCS, School of Physical Science and Technology, Nanjing Normal University, Nanjing 210023, P. R. China

Supporting Information

ABSTRACT: A new compound, $\{[Co(bmzbc)_2]\cdot 2DMF\}_n$ (**JXNU-1**, **JXNU** denotes Jiangxi Normal University), based on the 4-(benzimidazole-1-yl)benzoate ($bmzbc^-$) ligand has been synthesized and structurally characterized. The Co(II) ions are bridged by the rod-like $bmzbc^-$ ligands to give a two-dimensional (2D) sheet wherein the Co(II) ions are spatially separated from each other by the long $bmzbc^-$ rods. The 2D sheets are further stacked into a 3D framework with 1D channels occluding the guest DMF molecules. Detailed magnetic studies show that the individual octahedral Co(II) ions in **JXNU-1** exhibit field-induced slow magnetic relaxation, which is characteristic behavior of single-ion magnets (SIMs). The rarely observed positive value of zero-field splitting (ZFS) parameter D for the Co(II) ion in **JXNU-1** demonstrates that **JXNU-1** is a unique example of Co(II)-based SIMs with easy-plane anisotropy, which is also confirmed by the calculations. The microporous nature of **JXNU-1** was established by measuring CO_2 sorption isotherms. The abrupt changes observed in the C_3H_8 and C_2H_6 adsorption isotherms indicate that a structural transformation occurred in the gas-loading process. The long connection between the magnetic metal centers in **JXNU-1** meets the requirements for construction of porosity and SIM in a well-defined network, harmoniously providing a good candidate of functional molecular materials exhibiting SIM and porosity.

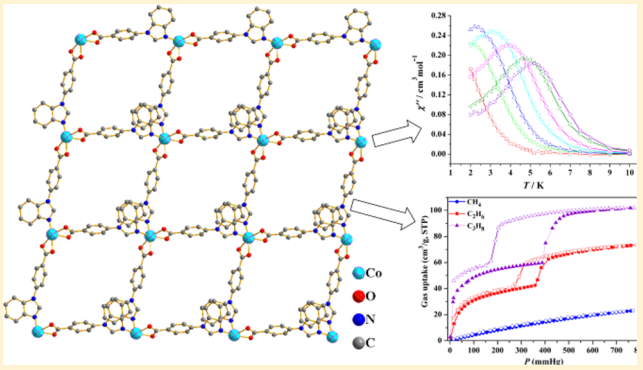

INTRODUCTION

Single-ion magnets (SIMs) with slow magnetic relaxation stemming from a single paramagnetic ion are an important type of single-molecule magnets (SMMs).[1] Since the SIM behavior has been observed first in the mononuclear $Tb(III)Pc_2$ compound,[2] the research of the lanthanide-based SIMs has been extensively studied because these magnetic systems provide elegant models to understand quantum phenomenon at molecular level and have potential applications in quantum computing and high-density information storage.[3] Thus, many lanthanide SIMs have been documented in the past ten years.[4] Very recently, a few examples of SIM based on the 3d transition-metal ions have been reported due to the single-ion anisotropy.[5] It has been reported that the single lanthanide ions spatially separated in a coordination polymer can show slow magnetic relaxation arising from the single-ion magnetic anisotropy.[6] Similarly, if the 3d transition-metal ions with suitable local magnetic anisotropy in an appropriate ligand field are magnetically isolated in a well-defined coordination network, can it possess SIM behavior resulting from the single-ion anisotropy? To realize this, a long spatial ligand of 4-(benzimidazole-1-yl)benzoic acid (Hbmzbc) was synthesized (Supporting Information). The Hbmzbc ligand is suitable as a bridging ligand with diverse configurations, as a result of the free rotation of the C—N single bond between the benzene and benzimidazole moieties. The carboxylate group and the N donor atom are arranged at the head and tail of the ligand, respectively, which can effectively separate the metal centers from each other in a polymeric structure.

However, the porous coordination polymers or metal−organic frameworks (MOFs) consist of metal ions and organic linkers within the frameworks and have shown great promise as functional solid materials for gas storage and separation, catalysis, and sensing.[7] The three-dimensional (3D) frameworks have afforded the greatest diversity of the porous coordination polymers due to their structural rigidity and porous character. However, research on 2D porous coordination polymers has been significantly lagging behind that of 3D porous coordination polymers. Indeed, the 2D structures can be stacked into 3D dense frameworks with porosities exhibiting adsorption properties.[8]

Received: August 27, 2015

DOI: 10.1021/acs.inorgchem.5b02324
Inorg. Chem. XXXX, XXX, XXX−XXX

For porosity and long-range magnetic ordering, they are inimical based on the fact that the former requires long connections between the metal centers, while the latter needs short ones.[9] However, concerning the porosity and SIM in a network, both of them require long connection between metal centers. Following this approach, we choose the cobalt(II) ion with large magnetic anisotropy as a metal center and the rod-spaced Hbmzbc ligand as long connection for construction of the multifunctional material exhibiting SIM and porosity. A novel compound, $\{[Co(bmzbc)_2]\cdot 2DMF\}_n$ (**JXNU-1**), is reported in this contribution. The SIM-type slow magnetic relaxation and interesting adsorption properties have been observed in compound **JXNU-1**. Thus, it is a rare example of functional molecular materials exhibiting SIM and porosity harmoniously.

EXPERIMENTAL SECTION

Chemicals. All chemicals were of reagent grade and used as commercially obtained. The starting material 4-(benzimidazole-1-yl)benzoic acid (Hbmzbc) was prepared following a modified known procedure.[10] It should be noted that our synthetic method for Hbmzbc is different from that of the reported method.[11]

Physical Measurements. Elemental analyses were carried out on an Elementar Vario EL III analyzer and IR spectra (KBr pellets) were recorded on PerkinElmer Spectrum One. Elemental analyses were carried out on Elementar PerkinElmer 2400CHN microanalyzer. Thermogravimetric analyses were carried out on a PE Diamond TG/DTA unit at a heating rate of 10 °C/min under a nitrogen atmosphere. Powder X-ray diffraction patterns were performed on a Rigaku Miniflex Π powder diffractometer using Cu−Kα radiation (λ = 1.5418 Å). Magnetic measurements were carried out on crystalline samples with a Quantum Design MPMS-XL5 SQUID magnetometer in the temperature range of 2−300 K. Diamagnetic corrections were estimated from Pascal's constants for all constituent atoms.[12] Gas sorption isotherms were measured using a Micromeritics ASAP2020 gas adsorption instrument.

Synthesis of $\{[Co(bmzbc)_2]\cdot 2DMF\}_n$ (JXNU-1). A mixture of $Co(NO_3)_2\cdot 6H_2O$ (0.0291 g, 0.1 mmol), 4-(benzimidazole −1-yl)benzoic acid (0.0714 g, 0.3 mmol), methylamine (0.05 mL) and DMF (10 mL) was sealed in a Teflon-lined stainless steel autoclave, which was heated at 120 °C for 72 h under autogenous pressure. The resulting mixture was cooled naturally to obtain the purple crystals (yield: 0.018 g, 62% on the basis of Co). Anal. Calcd. for $C_{34}H_{32}N_6O_6Co$ (679.59): C, 60.09; H, 4.75; N, 12.37%. Found: C, 60.13; H, 4.79; N, 12.48%. Main IR features (KBr pellet, cm^{-1}): 3290 (m), 3130 (w), 2965 (w), 1660 (s), 1604 (s), 1540 (s), 1517 (m), 1502 (w), 1478 (w), 1460 (m), 1425 (s), 1408 (w), 1385 (m), 1323 (m), 1298 (m), 1236 (s), 1176 (w), 1103 (w), 1061 (w), 1012 (m), 987 (m), 940 (w), 87 (w), 859 (m),789 (s), 778 (w), 747 (m), 736 (w), 704 (m), 652 (w), 622 (w), 583 (w), 531 (w), 493 (m), 429 (w).

X-ray Crystallography. X-ray diffraction data were collected on a Bruker Apex II CCD diffractometer equipped with a graphite-monochromated Mo−Kα radiation (λ = 0.710 73 Å) at 100 K. Data reduction was performed using SAINT and corrected for Lorentz and polarization effects. Adsorption corrections were applied using the SADABS routine.[13] The structure was solved by the direct methods and successive Fourier difference syntheses, and refined by the full-matrix least-squares method on F^2 (SHELXTL Version 5.1).[14] All non-hydrogen atoms are refined with anisotropic thermal parameters. Hydrogen atoms were assigned to calculated positions. The DMF solvents were highly disordered, and attempts to locate and refine the solvent peaks were unsuccessful. The diffused electron densities resulting from these residual solvents were removed from the data using the SQUEEZE routine of PLATON[15] and refined further using the data generated. Two guest DMF molecules per formula unit are observed in the channels, as established by elemental and thermogravimetric analyses. The R_1 values are defined as $R_1 = \Sigma||F_o| - |Fc||/\Sigma|F_o|$ and $wR_2 = \{\Sigma[w(F_o^2 - F_c^2)^2]/\Sigma[w(F_o^2)^2]\}^{1/2}$. Details of the crystal parameters, data collection, and refinement are summarized in Table 1. Important bond lengths are listed in Table S1. More details on the crystallographic data are given in the X-ray crystallographic files in CIF format.

Table 1. Crystallographic Data for Compound JXNU-1[a]

compound	JXNU-1
formula	$C_{34}H_{32}N_6O_6Co$
fw	679.59
temp (K)	100
cryst syst	monoclinic
space group	*C*2/*c*
Z	4
a (Å)	17.815(5)
b (Å)	15.672(4)
c (Å)	14.185(6)
α (deg)	90
β (deg)	124.964(3)
γ (deg)	90
V (Å^3)	2729.2(7)
D_{calcd} (g•cm^{-3})	1.391
μ (mm^{-1})	0.583
no. of reflns collected	9607
independent reflns	3729
obsd. reflns. ($I > 2\sigma(I)$)	2535
F(000)	1412
GOF on F^2	1.009
2θ range [°]	1.98 to 27.62
R[int]	0.0488
*R*1, wR_2 [$I > 2\sigma(I)$]	0.0708, 0.1878
*R*1, wR_2 (all data)	0.1026, 0.2026
CCDC number	1420038

[a] $R_1 = \Sigma||Fo| - |Fc||/\Sigma|Fo|$ and $wR_2 = \{\Sigma[w(Fo^2 - Fc^2)^2]/\Sigma[w(Fo^2)^2]\}^{1/2}$.

Theoretical Calculations. Complete active space second-order perturbation theory (CASPT2) considering the effect of the dynamical electronic correlation based on complete-active-space self-consistent field (CASSCF) using the *MOLCAS 7.8* program package[16] was performed on the model structure of compound **JXNU-1** to obtain the parameters *D* and *E*. For the first CASSCF calculation, the basis sets for all atoms are atomic natural orbitals from the MOLCAS ANO-RCC library: ANO-RCC-VTZP for magnetic center ion Co(II); VTZ for close O and N; VDZ for distant atoms. The calculations employed the second order Douglas−Kroll−Hess Hamiltonian, where scalar relativistic contractions were taken into account in the basis set. After that, the effect of the dynamical electronic correlation was applied using CASPT2. And then, the spin−orbit coupling was handled separately in the restricted active space state interaction (RASSI-SO) procedure. The active electrons in 10 active spaces include all seven 3*d* electrons, and the mixed spin-free states are 50 (all from 10 quadruplets; all from 40 doublets).

RESULTS AND DISCUSSION

Solvothermal reaction of $Co(NO_3)_2$, Hbmzbc, and methylamine in DMF solvent afforded purple crystals of $\{[Co(bmzbc)_2]\cdot 2DMF\}_n$ (**JXNU-1**) (Table 1). Half a Co(II) ion and one $bmzbc^-$ ligand, together with an additional disordered DMF molecule are in the asymmetric unit. The Co atom is located on a 2-fold rotation axis and bonded to four carboxylate O atoms from two $bmzbc^-$ ligands and two benzimidazole N atoms from another two $bmzbc^-$ ligands in an octahedral coordination geometry (Figure 1a). Two N atoms and two O atoms (O1 and O1A) form the equatorial plane and the

DOI: 10.1021/acs.inorgchem.5b02324
Inorg. Chem. XXXX, XXX, XXX−XXX

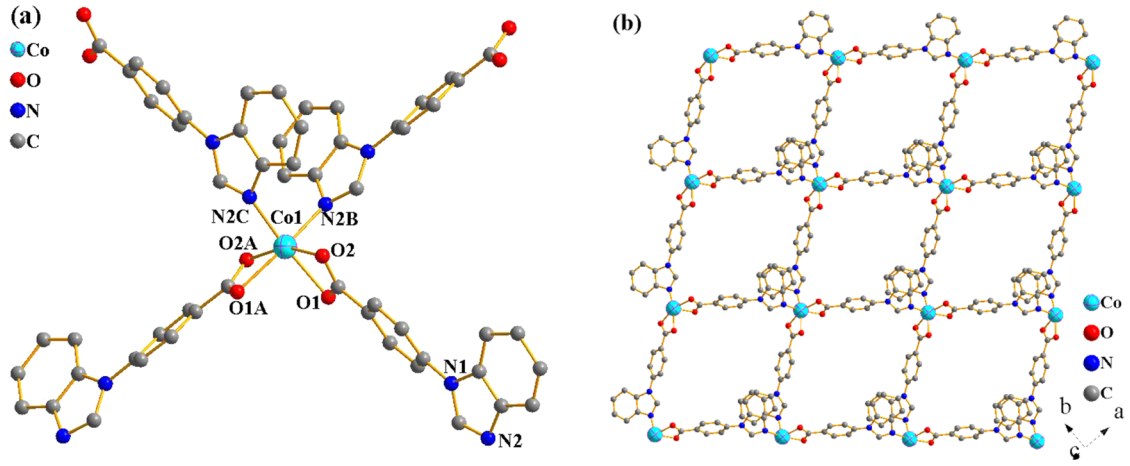

Figure 1. (a) Coordination environment of Co(II) center and (b) 2D sheet of **JXNU-1**.

remaining two O atoms take up the axial positions. The axial Co—O bond distances [2.109(2) Å] are slightly shorter than the equatorial Co—O/N bond distances [2.185(3) and 2.115(3) Å] (Table S1), indicating a slightly compressed [CoN_2O_4] octahedron. These bond distances are normal and comparable to those in other Co(II) compounds.[17] Additionally, the equatorial O/N—Co—O/N bond angles varying from 87.09(15) to 95.07(10)° and the axial O—Co—O bond angle of 159.97(14) ° (Table S1), deviate from the corresponding angles of 90 and 180°, respectively, of an ideal octahedron. All these structural geometric parameters indicate an overall rhombic (C_{2v}) distortion of the octahedral metal environment for Co atom.

Each Co(II) ion is surrounded by four $bmzbc^-$ ligands, which link the Co(II) ions to give a 2D sheet running along *ab* plane (Figure 1b). The 2D sheet features the metal−organic squares with the Co···Co separation of 11.86 Å. The 2D sheets are stacked along *c* axis in a repeated—[A−B]—staggered configuration forming a 3D framework (Figure 2). Careful examination of the crystal packing indicates the shortest interlayered Co···Co separation of 8.32 Å (Figure S1), indicative of an isolated magnetic environment for the Co(II) ions. The 3D packing possesses square 1D open channels with window size of about 7.1 × 7.1 $Å^2$, wherein the guest DMF molecules reside in.

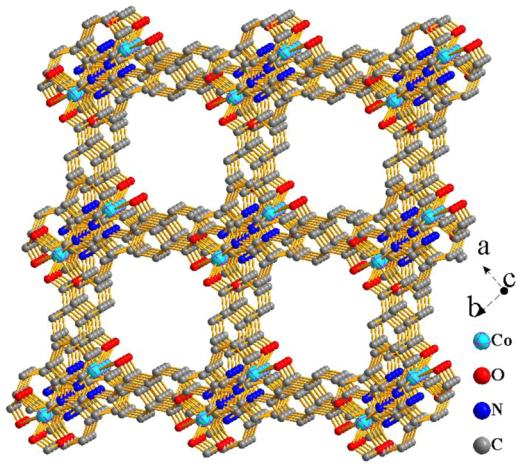

Figure 2. View of the 3D framework of **JXNU-1** along the *c* axis showing the 1D open channels.

The direct current (dc) magnetic susceptibility of **JXNU-1** was collected in an applied magnetic field of 1 kOe. The plot of $\chi_M T$ (χ_M is the molar magnetic susceptibility per Co(II)) versus T is depicted in Figure 3. Above 110 K, the $\chi_M T$ value (2.88

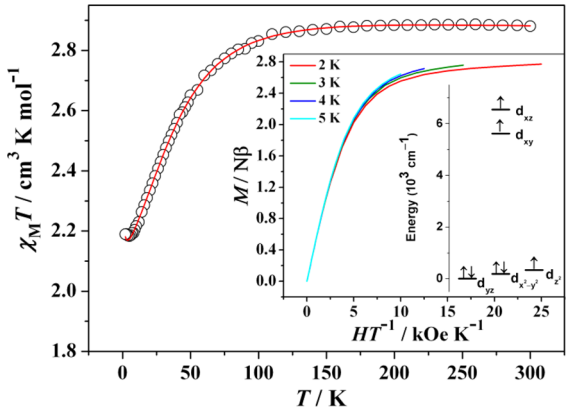

Figure 3. $\chi_M T$ versus T plot for **JXNU-1**. Solid line is the best fit obtained with the *PHI* program. Inset: Field dependence of the magnetization measured at different temperatures and calculated energy splitting of d orbits for the Co(II) ion.

cm^3 K mol^{-1}) is a constant and much higher than the theoretical spin-only value of 1.87 cm^3 K mol^{-1} for a Co(II) ion (S = 3/2 and g_0 = 2.0). However, comparable large room temperature $\chi_M T$ values have been reported for other Co(II) compounds.[18] An effective g_{eff} tensor of value of 2.47 can be deduced from the room temperature $\chi_M T$ value, which is larger than the spin-only value of g_0, indicating the considerable orbital contributions to the spin-only value. $\chi_M T$ value sharply decreases upon cooling below 100 K to a value of 2.17 cm^3 K mol^{-1} at 2 K, indicative of a significant zero-field splitting (ZFS).

$$H = D[\hat{S}_z^2 - S(S+1)/3] + E(\hat{S}_x^2 - \hat{S}_y^2) + \mu_B g \hat{S} \hat{B} \quad (1)$$

In order to describe the magnetic anisotropy qualitatively, the spin Hamiltonian of eq 1 (where D is the axial ZFS parameter, E is the rhombic or transverse ZFS parameter, S is the spin operator, μ_B is the Bohr magneton, and B is the

DOI: 10.1021/acs.inorgchem.5b02324
Inorg. Chem. XXXX, XXX, XXX−XXX

magnetic field vector, respectively), which takes into account the axial (D) and rhombic (E) magnetic anisotropies, was used. Some simplification of the structure (Figure S2) was performed and calculations were performed with the *MOLCAS 7.8* program.[16] The calculation results gave D = 62.6 cm^{-1}, E = 13.4 cm^{-1}, g_x = 2.055, g_y = 2.362, and g_z = 2.849 (Figure S3). According to the calculation results, the energy splitting of d orbits (Figure 3 inset) and easy axis for the Co(II) ion were successfully obtained. The direction of magnetic axis is approximately perpendicular to the C_2-axis that passed through the Co atom (Figure 4).

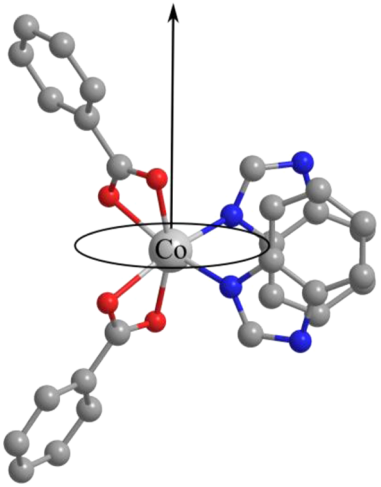

Figure 4. Scheme of the local hard axis and the easy plane of the ground state on Co(II) in **JXNU-1**.

Moreover, the experimental $\chi_M T$ versus T plot was fit using the *PHI* program,[19] giving D = 53.2 cm^{-1}, E = 7.5 cm^{-1}, g = 2.46 (Figure 3). The field dependence of the magnetization reveals a relatively rapid increase of the magnetization at low field followed by a slow linear increase at high field in the low temperatures (Figure 3 inset). The experimental field dependence of magnetization data were analyzed using *PHI* program adopting the spin Hamiltonian of eq 1, affording D = 60.4 cm^{-1}, E = 8.0 cm^{-1}, and g = 2.42 (Figure S4). The fitting D and E values are comparable and slightly smaller than the above calculated values. The cobalt(II)-based SMMs with a positive D value, which are different the traditional SMMs with a negative D valule, are rarely documented.[20] The D value fitted from the experimental $\chi_M T$ versus T plot is larger than that of 27.9 cm^{-1} in a metallamacrocycle compound wherein the Co(II) ions are alternately separated by two Li^+ cations that bridged by the γ-cyclodextrins,[21] but smaller than that of 91.0 cm^{-1} in the 1D cobalt(II) compound.[22]

The alternating-current (ac) magnetic susceptibility at various frequencies and temperatures were collected at a zero dc field with an ac field of 2.5 Oe. No out-of-phase (χ'') signal can be observed for **JXNU-1** (Figure S5), suggesting a fast quantum tunneling of the magnetization (QTM). Both in-phase (χ') and out-of-phase (χ'') susceptibilities show significant frequency dependence below 9 K, when a 2 kOe dc field was applied (Figure 5). The χ'' peaks can be observed in the frequency region of 50−1399 Hz. Arrhenius analysis of the χ'' peaks from the high temperature regime of the relaxation gave the anisotropy energy barrier U_{eff} of 11.8 K (8.7 cm^{-1}) with a pre-exponential factor value τ_0 of 1.3 × 10^{-5} s (Figure S6). The U_{eff} value is higher than that of (5.1 cm^{-1}) dicyanamide-bridged 2D coblat(II) compound under 1 kOe dc field.[23]

Interestingly, the Cole−Cole plots measured at 2 and 3 K in the 2 kOe dc field exhibit obvious two-step magnetic relaxation properties (Figure 6): the left and right parts of the Cole−Cole

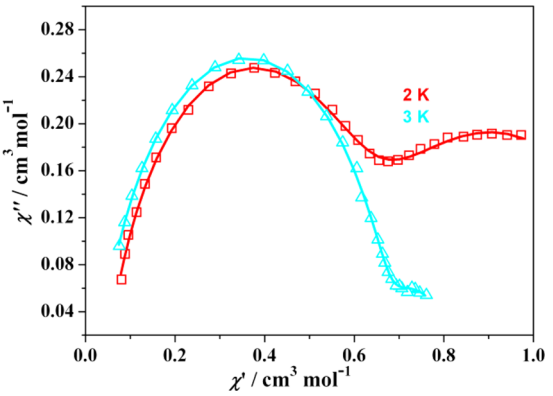

Figure 6. Cole−Cole plots at 2 and 3 K under 2 kOe for **JXNU-1** (The solid lines represent the best fitting with the sum of two modified Debye functions).

curve correspond to the fast relaxation phase (FR) and the slow relaxation phase (SR), respectively. The two steps of magnetic relaxation processes can be fitted with the sum of two modified Debye functions (Equation S1).[24] The fitting results are depicted as Figures 6 and S7, and summarized in Table S2. The α_1 values (0.375 and 0.210 for 2 and 3 K, respectively) are

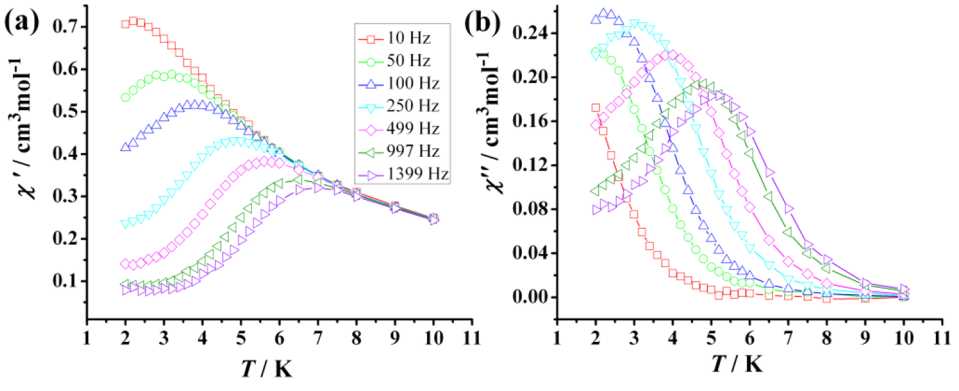

Figure 5. Temperature dependence of the in-phase (a) and out-of phase (b) ac susceptibility signals under 2 kOe dc field with an ac field of 2.5 Oe.

DOI: 10.1021/acs.inorgchem.5b02324
Inorg. Chem. XXXX, XXX, XXX−XXX

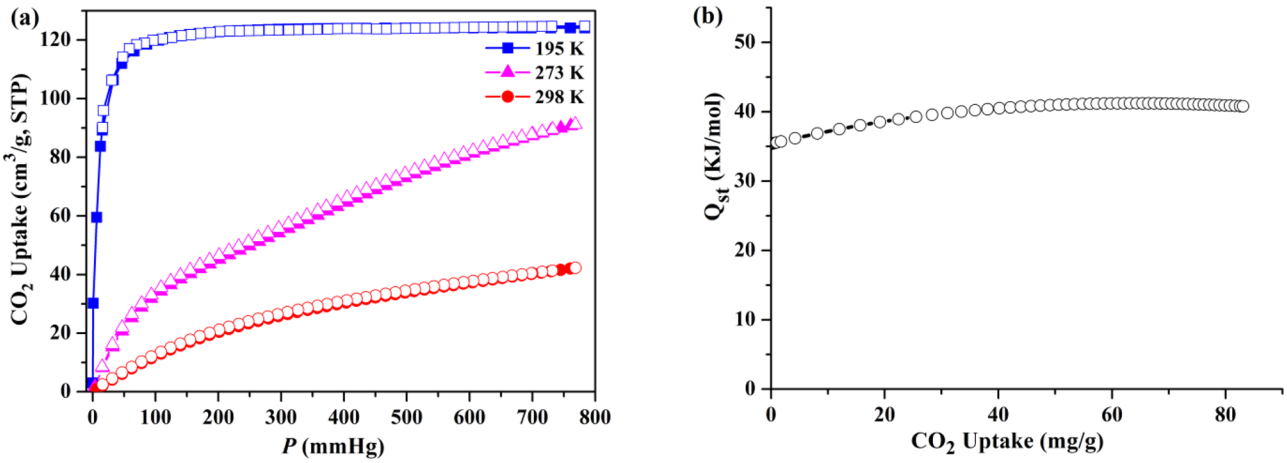

Figure 7. (a) CO_2 sorption isotherms at 195, 273, and 298 K (solid symbols: adsorption, open symbols: desorption) and (b) the isosteric heats of adsorption of CO_2.

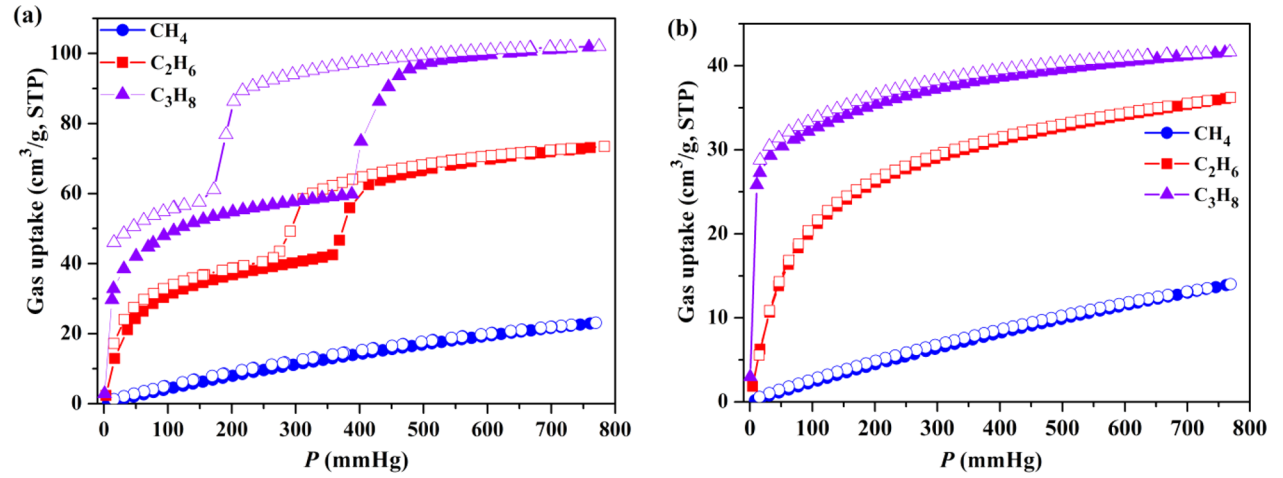

Figure 8. CH_4, C_2H_6, and C_3H_8 sorption isotherms at 273 K (a) and 298 K (b) (solid symbols: adsorption, open symbols: desorption).

obviously larger than the coresponding α_2 values (0.149 and 0.155 for 2 and 3 K, respectively), suggesting that the SR phase has a relatively narrower distribution of the relaxation time with respect to the FR phase. As mentioned above, there is only one kind of Co(II) ion in **JXNU-1**, so the field-inducing role is ascribed to the two-step magnetic relaxation.[25]

The phase purity of **JXNU-1** was confirmed by elemental analysis and powder X-ray diffraction (PXRD) (Figure S8). Solvent accessible volume, calculated using the PLATON routine,[26] is 37.1% of the total crystal volume. The thermogravimetric profile of **JXNU-1** showed that the loss of DMF solvents occurs in two steps (Figure S9). The release of DMF molecules commences at 40 °C and is completed by 205 °C (observed 21.11%, calculated 21.14%). After removal of the guest DMF molecules, no obvious weight loss occurred below 330 °C.

As verified by PXRD (Figure S8), the activated sample retained the crystallinity after being evacuated under high vacuum for 10 h at 150 °C. The permanent porosity of **JXNU-1** was established by measuring CO_2 sorption isotherms (Figure 7a). The desolvated **JXNU-1a** shows a significant CO_2 adsorption at 195 K, and the isotherm shows a very sharp uptake at $P/P_0 < 0.15$, confirming the presence of permanent microporosity. The CO_2 absorption exhibits a type-I isotherm,[27] with a measured saturated adsorption amount of 124 $cm^3(STP)\ g^{-1}$ (5.5 mmol g^{-1}) at 195 K. The pore volume is 0.31 $cm^3\ g^{-1}$ calculated by assuming liquid filling of CO_2 at saturated state, which matches well with the value of 0.34 $cm^3\ g^{-1}$ estimated from the crystal data. Meanwhile, CO_2 uptakes at 273 and 298 K are 91 and 42 $cm^3\ g^{-1}$, respectively, demonstrating **JXNU-1a** as a solid material for potential CO_2 capture. The existence of extensive aromatic rings on the pore surfaces would largely account for the high CO_2 uptake. The coverage-dependent adsorption enthalpy of **JXNU-1a** for CO_2 was calculated based on the viral method from fits of their adsorption isotherms at 273 and 298 K (Figure S10).[28] The isosteric heat of adsorption Q_{st} at zero loading was calculated to be 35.4 kJ mol^{-1} (Figure 7b), which is comparable to those observed in other compounds, such as **HKUST-1** (35 kJ mol^{-1})[29] and **MOF-5** (34 kJ mol^{-1}),[30] but is larger than those of **NOTT-140** (25 kJ mol^{-1})[31] and **Tripp-1-Co** (25.6 kJ mol^{-1}).[32] In contrast, the N_2 uptake of **JXNU-1a** at 77 K is very low with only 15.5 $cm^3\ g^{-1}$ at P/P_0 = 0.90 (Figure S11), indicating that N_2 molecules are unable to interact with the pores.

Adsorption isotherms for C_1 to C_3 paraffins were measured at 273 and 298 K (Figure 8). As shown in Figure 8a, **JXNU-1a** takes up less CH_4 (23 $cm^3\ g^{-1}$, 273 K) at 1 atm, but adsorbs significant amounts of C_3H_8 and C_2H_6, with the uptakes of 118 and 73 $cm^3\ g^{-1}$ (273 K) at 1 atm. The C_3H_8 uptake is higher

DOI: 10.1021/acs.inorgchem.5b02324
Inorg. Chem. XXXX, XXX, XXX−XXX

than that of the recently reported Zn-pyrazole-adenine framework (88 cm^3 g^{-1} at 273 K).[33] It is interesting that the C_3H_8 and C_2H_6 isotherms at 273 K exhibit an abrupt increase at P/P_0 = 0.51 and 0.47, respectively. Additionally, large hysteretic desorption behavior is observed in the isotherms of C_3H_8 and C_2H_6 (Figure 8a), suggesting the framework flexibility and the existence of molecular gates.[34] Such behavior can be attributed to the association with a structural transformation from the guest-free **JXNU-1a** to gas-loaded **JXNU-1g**. The less porous **JXNU-1a** can be expanded to more porous **JXNU-1g** once gas molecules have been gradually loaded into the pores. However, this adsorption behavior is different from that of the reported interdigitated 2D framework wherein a structural transformation from a nonporous to a microporous phase is observed.[35] With increasing temperature, the adsorptions of C_3H_8 and C_2H_6 gradually decrease but become more reversible (Figure 8b). It should be noted that the isotherms for C_3H_8 and C_2H_6 at 298 K and for CO_2 and CH_4 at all testing temperatures exhibit no hysteretic profile (Figure 7a and Figure 8b). As is well-known, the adsorption properties are related to the interactions between gas molecules with the frameworks, and the gate-opening pressure is sensitive to the property of the gas adsorbed. The larger gas molecules (such as C_3H_8 and C_2H_6) commonly have strong interactions with the host frameworks, thus the hysteresis will be obvious, whereas at higher temperatures such phenomena will not be very obvious or not be observed at all due to the lower host–guest interactions and much higher gate-opening pressure.

CONCLUSIONS

A novel cobalt(II) compound, $\{[Co(bmzbc)_2]\cdot 2DMF\}_n$ (**JXNU-1**), displays field-induced slow magnetic relaxation resulting from the anisotropic Co(II) ions which behave as SIM units. The rod-like $bmzbc^-$ ligand spatially separates the magnetic ions in a well-defined network, which provides an approach to obtaining independent single-ion magnets. Moreover, the 3D porous packing framework shows abrupt changes in its adsorption isotherms with guest-dependent gate-opening pressure. This work demonstrates a rare example of bifunctional materials, which opens up new opportunities in the preparation of the multifunctional molecular materials with SIM and porosity.

ASSOCIATED CONTENT

Supporting Information

The Supporting Information is available free of charge on the ACS Publications website at DOI: 10.1021/acs.inorgchem.5b02324.

Experimental details, structural and magnetic characterization, theoretical calculation (PDF)

X-ray crystallographic files in CIF format, TGA curve, and PXRD (CIF)

AUTHOR INFORMATION

Corresponding Authors

*E-mail: ylwangchem@gmail.com (Y.-L.W.).

*Fax: +86-791-88336372. E-mail: qyliuchem@hotmail.com (Q.-Y.L.).

Notes

The authors declare no competing financial interest.

ACKNOWLEDGMENTS

This work was supported by the NNSF of China (Grants 21361011, 21101081, and 21561015), the NSF of Jiangxi (Grant 20151BAB203002), the Young Scientist Training Project of Jiangxi Province (Grant 20153BCB23017), and the project of Education Department of Jiangxi (Grant GJJ14235).

REFERENCES

(1) Gatteschi, D.; Sessoli, R.; Villain, J. *Molecular Nanomagnets*; Oxford University Press: Oxford, UK, 2006.

(2) Ishikawa, N.; Sugita, M.; Ishikawa, T.; Koshihara, S.; Kaizu, Y. *J. Am. Chem. Soc.* **2003**, *125*, 8694–8695.

(3) Bartolomé, J.; Luis, F.; Fernandez, J. F., Eds. *Molecular Magnets: Physics and Aplications*; Springer-Verlag: Berlin, 2014.

(4) (a) Sorace, L.; Benelli, C.; Gatteschi, D. *Chem. Soc. Rev.* **2011**, *40*, 3092–3104. (b) Woodruff, D. N.; Winpenny, R. E. P.; Layfield, R. A. *Chem. Rev.* **2013**, *113*, 5110–5148. (c) Habib, F.; Murugesu, M. *Chem. Soc. Rev.* **2013**, *42*, 3278–3288. (d) Luzon, J.; Sessoli, R. *Dalton Trans.* **2012**, *41*, 13556–13567.

(5) (a) Jurca, T.; Farghal, A.; Lin, P. H.; Korobkov, I.; Murugesu, M.; Richeson, D. S. *J. Am. Chem. Soc.* **2011**, *133*, 15814–15817. (b) Zadrozny, J. M.; Long, J. R. *J. Am. Chem. Soc.* **2011**, *133*, 20732–20734. (c) Habib, F.; Luca, O. R.; Vieru, V.; Shiddiq, M.; Korobkov, I.; Gorelsky, S. I.; Takase, M. K.; Chibotaru, L. F.; Hill, S.; Crabtree, R. H.; Murugesu, M. *Angew. Chem., Int. Ed.* **2013**, *52*, 11290–11293. (d) Zhu, Y. Y.; Zhang, Y. Q.; Yin, T. T.; Gao, C.; Wang, B. W.; Gao, S. *Inorg. Chem.* **2015**, *54*, 5475–5486. (e) Nemec, I.; Marx, R.; Herchel, R.; Neugebauer, P.; Slageren, J.; Trávníček, Z. *Dalton Trans.* **2015**, *44*, 15014–15021. (f) Bar, A. K.; Pichon, C.; Sutter, J.-P. *Coord. Chem. Rev.* **2015**, DOI: 10.1016/j.ccr.2015.06.013.

(6) (a) Yin, D. D.; Chen, Q.; Meng, Y. S.; Sun, H. L.; Zhang, Y. Q.; Gao, S. *Chem. Sci.* **2015**, *6*, 3095–3101. (b) Liu, S. J.; Zhao, J. P.; Song, W. C.; Han, S. D.; Liu, Z. Y.; Bu, X. H. *Inorg. Chem.* **2013**, *52*, 2103–2109.

(7) (a) Furukawa, H.; Cordova, K. E.; O'Keeffe, M.; Yaghi, O. M. *Science* **2013**, *341*, 1230444–1230444. (b) Zhang, J. P.; Zhang, Y. B.; Lin, J. B.; Chen, X. M. *Chem. Rev.* **2012**, *112*, 1001–1033. (c) Li, J. R.; Sculley, J.; Zhou, H. C. *Chem. Rev.* **2012**, *112*, 869–932.

(8) (a) Tanaka, D.; Nakagawa, K.; Higuchi, M.; Horike, S.; Kubota, Y.; Kobayashi, T. C.; Takata, M.; Kitagawa, S. *Angew. Chem., Int. Ed.* **2008**, *47*, 3914–3918. (b) Horike, S.; Tanaka, D.; Nakagawa, K.; Kitagawa, S. *Chem. Commun.* **2007**, 3395–3397.

(9) Wang, Z.; Zhang, B.; Fujiwara, H.; Kobayashi, H.; Kurmoo, M. *Chem. Commun.* **2004**, 416–417.

(10) Wang, Y.-L.; Fu, J.-H.; Wei, J.-J.; Xu, X.; Li, X.-F.; Liu, Q.-Y. *Cryst. Growth Des.* **2012**, *12*, 4663–4668.

(11) Aijaz, A.; Lama, P.; Saudo, E. C.; Mishra, R.; Bharadwaj, P. K. *New J. Chem.* **2010**, *34*, 2502–2514.

(12) Kahn, O. *Molecular Magnetism*; VCH: Weinheim, Germany, 1993.

(13) *APEX2, SADABS and SAINT*; Bruker AXS Inc.: Madison, WI, 2008.

(14) Sheldrick, G. M. *Acta Crystallogr., Sect. A: Found. Crystallogr.* **2008**, *A64*, 112–122.

(15) Van der Sluis, P.; Spek, A. L. *Acta Crystallogr., Sect. A: Found. Crystallogr.* **1990**, *46*, 194–201.

(16) *MOLCAS: A Program Package for Computational Chemistry*: Karlstrom, G.; Lindh, R.; Malmqvist, P. A.; Roos, B. O.; Ryde, U.; Veryazov, V.; Widmark, P. O.; Cossi, M.; Schimmelpfennig, B.; Neogrady, P.; Seijo, L. *Comput. Mater. Sci.* **2003**, *28*, 222–239.

(17) (a) Zeng, M.-H.; Zheng, Y.; Tan, Y.-X.; Zhang, W.-X.; He, Y.-P.; Kurmoo, M. *J. Am. Chem. Soc.* **2014**, *136*, 4680–4688. (b) Li, B.; Li, Z.; Wei, R.-J.; Yu, F.; Chen, X.; Xie, Y.-P.; Zhang, T.-L.; Tao, J. *Inorg. Chem.* **2015**, *54*, 3331–3336. (c) Chen, X.; Li, Z.; Wei, R.-J.; Li, B.; Zhang, T.-L.; Tao, J. *New J. Chem.* **2015**, *39*, 7333–7339.

(18) (a) Huang, X. C.; Zhou, C.; Shao, D.; Wang, X. Y. *Inorg. Chem.* **2014**, *53*, 12671–12673. (b) Zadrozny, J. M.; Liu, J.; Piro, N. A.; Chang, C. J.; Hill, S.; Long, J. R. *Chem. Commun.* **2012**, *48*, 3927–

DOI: 10.1021/acs.inorgchem.5b02324
Inorg. Chem. XXXX, XXX, XXX–XXX

3929. (c) Poulten, R. C.; Page, M. J.; Algarra, A. G.; Le Roy, J. J.; López, I.; Carter, E.; Llobet, A.; Macgregor, S. A.; Mahon, M. F.; Murphy, D. M.; Murugesu, M.; Whittlesey, M. K. *J. Am. Chem. Soc.* **2013**, *135*, 13640−13643.
(19) Chilton, N. F.; Anderson, R. P.; Turner, L. D.; Soncini, A.; Murray, K. S. *J. Comput. Chem.* **2013**, *34*, 1164−1175.
(20) (a) Vallejo, J.; Castro, I.; Ruiz-García, R.; Cano, J.; Julve, M.; Lloret, F.; De Munno, G.; Wernsdorfer, W.; Pardo, E. *J. Am. Chem. Soc.* **2012**, *134*, 15704−15707. (b) Huang, W.; Liu, T.; Wu, D.; Cheng, J.; Ouyang, Z. W.; Duan, C. *Dalton Trans.* **2013**, *42*, 15326−15331. (c) Herchel, R.; Váhovská, L.; Potočňák, I.; Trávníček, Z. *Inorg. Chem.* **2014**, *53*, 5896−5898. (d) Gómez-Coca, S.; Urtizberea, A.; Cremades, E.; Alonso, P. J.; Camón, A.; Ruiz, E.; Luis, F. *Nat. Commun.* **2014**, *5* (4300), 1−8.
(21) Nedelko, N.; Kornowicz, A.; Justyniak, I.; Aleshkevych, P.; Prochowicz, D.; Krupiński, P.; Dorosh, O.; Ślawska-Waniewska, A.; Lewiński, J. *Inorg. Chem.* **2014**, *53*, 12870−12876.
(22) Zhu, Y. Y.; Zhu, M. S.; Yin, T. T.; Meng, Y. S.; Wu, Z. Q.; Zhang, Y. Q.; Gao, S. *Inorg. Chem.* **2015**, *54*, 3716−3718.
(23) Palion-Gazda, J.; Klemens, T.; Machura, B.; Vallejo, J.; Lloret, F.; Julve, M. *Dalton Trans.* **2015**, *44*, 2989−2992.
(24) Grahl, M.; Kotzler, J.; Sessler, I. *J. Magn. Magn. Mater.* **1990**, *90-91*, 187−188.
(25) (a) Jeletic, M.; Lin, P. H.; Roy, J. J. L.; Korobkov, I.; Gorelsky, S. I.; Murugesu, M. *J. Am. Chem. Soc.* **2011**, *133*, 19286−19289. (b) Ruiz, J.; Mota, A. J.; Rodríguez-Diéguez, A.; Titos, S.; Herrera, J. M.; Ruiz, E.; Cremades, E.; Costes, J. P.; Colacio, E. *Chem. Commun.* **2012**, *48*, 7916−7918.
(26) Spek, A. L. *PLATON: A Multipurpose Crystallographic Tool*; Utrecht University: Utrecht, The Netherlands, 2001.
(27) Rouquerol, J.; Rouquerol, F.; Sing, K. W. *Adsorption by Powders and Porous Solids: Principles, Methodology and Applications*; Academic Press: London, 1999.
(28) Rowsell, J. L. C.; Yaghi, O. M. *J. Am. Chem. Soc.* **2006**, *128*, 1304−1315.
(29) Wang, Q. M.; Shen, D.; Bülow, M.; Lau, M. L.; Deng, S.; Fitch, F. R. N.; Lemcoffand, O.; Semanscin, J. *Microporous Mesoporous Mater.* **2002**, *55*, 217−230.
(30) Zhao, Z.; Li, Z.; Lin, Y. S. *Ind. Eng. Chem. Res.* **2009**, *48*, 10015−10020.
(31) Tan, C.; Yang, S.; Champness, N. R.; Lin, X.; Blake, A. J.; Lewis, W.; Schröder, M. *Chem. Commun.* **2011**, *47*, 4487−4489.
(32) Chen, K. J.; Perry, J. J., IV; Scott, H. S.; Yang, Q. Y.; Zaworotko, M. J. *Chem. Sci.* **2015**, *6*, 4784−4789.
(33) Fu, H. R.; Zhang, J. *Chem. - Eur. J.* **2015**, *21*, 5700−5703.
(34) (a) Horike, S.; Shimomura, S.; Kitagawa, S. *Nat. Chem.* **2009**, *1*, 695−704. (b) Wang, H. L.; Li, B.; Wu, H.; Hu, T. L.; Yao, Z. Z.; Zhou, W.; Xiang, S. C.; Chen, B. L. *J. Am. Chem. Soc.* **2015**, *137*, 9963−9970.
(35) Kitaura, R.; Seki, K.; Akiyama, G.; Kitagawa, S. *Angew. Chem., Int. Ed.* **2003**, *42*, 428−430.

DOI: 10.1021/acs.inorgchem.5b02324
Inorg. Chem. XXXX, XXX, XXX−XXX